30 May 1997

ELSEVIER

Chemical Physics Letters 270 (1997) 432–442

CHEMICAL PHYSICS LETTERS

Picosecond emission anisotropy decays of dimethyl aminobenzonitrile

J.J. Fisz [a,1], A. van Hoek [b]

[a] *Institute of Physics, N. Copernicus University, ul. Grudziądzka 5/7, PL 87-100 Toruń, Poland*

[b] *Molecular Physics Department, Agricultural University, Dreijenlaan 3, 6703 HA Wageningen, The Netherlands*

Received 9 January 1997; in final form 25 March 1997

Abstract

Picosecond polarized fluorescence experiments on DMABN (4-(dimethyl amino)benzonitrile) in polar solvents and toluene are reported. From the detected polarized fluorescence components emission anisotropy histograms are constructed and compared with the synthetic data simulated for the energy levels scheme in DMABN. For the short-wavelength emission of DMABN vibronic coupling between the close-lying S_1 and S_2 energy levels occurs and leads to a vibronically mixed polarization of the S_1 (F_B) fluorescence. Low initial values of the emission anisotropy decays for the long-wavelength (F_A) emission are observed. This observation can be explained by an assumption that the internal twisting of the amino group in DMABN changes the angular orientation of DMABN and by an assumption that the emission dipole moment in the F_A emission band is not parallel to the absorption dipole moment in the S_2 (^1L_a) absorption band. © 1997 Elsevier Science B.V.

1. Introduction

Since discovering the dual fluorescence of DMABN (4-(dimethyl amino)benzonitrile) [1–3] in polar solvents, this compound and its derivatives have become the subject of systematic experimental and theoretical investigations. In parallel to the studies on DMABN also other compounds showing dual emission, viz. indole, 1-naphthol, 1-naphthonitrile and 1-naphthylamine, were investigated in a systematic way (including fluorescence polarization experiments) (e.g. Refs. [4,5] and articles cited therein).

The model of "twisted intermolecular charge transfer" has been introduced in Refs. [6–8] to explain the dual fluorescence of DMABN and related compounds in polar solvents. The idea of the TICT model was extensively investigated on a number of different derivatives of DMABN (e.g. Refs. [9–13]). It has to be noted here that also other models have been offered in the literature to explain the mechanism leading to dual emission in DMABN and its derivatives (e.g. solute–solvent exciplex formation [15–17], the so-called "pseudo-Jahn–Teller coupling effect" model [18,19] or the recently proposed model that assumes a bending of the cyano group [20]).

The absorption band in DMABN consists of two overlapping bands: a highly intensive absorption band S_2 and the absorption band S_1 of low extinction coefficient. The S_1 and S_2 absorption bands in DMABN have been related by Lippert et al. [1,2] to the ^1L_b and ^1L_a absorption bands in benzene, respectively. The ^1L_a transition is polarized parallel to the long

[1] E-mail: jjfisz@phys.uni.torun.pl

PII S0009-2614(97)00388-6

molecular axis (the z-axis) of DMABN, while the ^1L_b is short-axis (the x-axis) polarized [1,2,7,10,14]. From excitation and emission wavelength-dependent steady-state polarized fluorescence measurements it has been concluded that the short-wavelength emission (F_B) in DMABN originates from the excited state of B symmetry (^1L_b-type state), whereas the second excited state which corresponds to the long-wavelength emission band (F_A) is of A symmetry (^1L_a-type state) [1,2]. Relatively small (or negative at the 0-0 transition) steady-state fluorescence anisotropy at low temperatures in the F_B emission band for DMABN and its derivatives has been explained in Ref. [7] to be the result of the vibronic coupling mechanism [21] between two close-lying excited states ^1L_b and ^1L_a. This feature was further discussed in Ref. [9] (see also Ref. [10]), on the basis of steady-state fluorescence polarization experiments on DMABN and its derivatives with different acceptor substituents, in polar solvents and at low temperatures.

Information about the vibronically mixed polarization of the short-wavelength emission of DMABN and other relevant systems, available in the literature, was deduced from steady-state fluorescence studies at low temperatures. For this reason we decided to explore this problem further by performing picosecond polarized fluorescence experiments on DMABN at much higher temperatures. In this work preliminary results are reported. We wish to discuss the results of picosecond polarized fluorescence experiments on DMABN in polar solvents and toluene. The measurements were performed for short emission wavelengths (in the F_B emission band) and for long emission wavelengths (in the F_A emission band or in the F_A band with a slight contribution of F_B emission). From the detected polarized fluorescence decays histograms of the emission anisotropy decays were constructed, which afterwards, were compared with the synthetic data generated under assumptions (a model) which correspond to the energy levels scheme of DMABN. Synthetic polarized fluorescence decays were obtained from the convolution of the model decays with the instrument response function which was detected at the same experimental conditions as the fluorescence decays of DMABN. Two cases were considered for the computer generated polarized decays. In the first case we assumed that there was no vibronic mixing of polarization in the F_B emission band. In the second case the vibronic coupling was included in the calculations and we assumed that an effective emission dipole moment in the F_B emission band made an angle of 45° (as an example) with the long molecular axis of DMABN, in order to reflect the vibronically mixed polarization of the F_B emission.

For the experimental cases reported in this work the vibronically mixed polarization in the F_B emission band is clearly manifested by positive initial values of the emission anisotropy histograms $r(t \approx 0)$. In the absence of vibronic coupling between the S_1 and S_2 excited states, the initial values of the emission anisotropy decays should be negative. Low values of $r(t \approx 0)$ for the long-wavelength emission are observed, as compared to the expected values (close to 0.4) according to the assumption that the absorption and emission dipoles are mutually parallel for the emission detected in the F_A band. This finding can be interpreted in such a way that the internal twisting in DMABN depolarizes the fluorescence, assuming that the F_A emission originates from a twisted form of DMABN, according to the TICT model. A rapid internal twisting can change the orientation of DMABN molecules. On the other hand, however, it is also possible that the emission dipole moment in DMABN in the F_A emission band is not parallel to the long molecular axis. This last conclusion can be argued by a relatively low value of the initial emission anisotropy of DMABN in glycerol, which at 526 nm is $r(t \approx 0) \approx 0.34$.

2. Experimental

Time-resolved fluorescence measurements on DMABN were carried out using time-correlated photon counting apparatus [22,23]. A mode-locked cw YLF laser (Coherent model Antares 76-YLF), which was equipped with an LBO frequency doubler to obtain an output of 527 nm wavelength, was used for the synchronous pumping of a cavity-dumped dye laser (Coherent model 701-2 CD). For experiments with excitations at 295 and 300 nm, the Rhodamine 6G dye laser was used and the output of the dye laser was frequency doubled using a BBO crystal (Gsänger). The repetition rate of the excitation pulses was 951 kHz, the duration about 4 ps FWHM and the pulse energy in the tens of pJ range. Fluores-

cence of the sample was focused on the cathode of a photomultiplier (Hamamatsu model 1645U). Single photon responses from the microchannel-plate photomultiplier were amplified by a wide band amplifier (Hewlett Packard model 8447F). The 1024 channels were used per experimental decay with a time spacing of 10 ps per channel. A photon frequency of 30 kHz was used to prevent pile-up distortion [22].

The measurements consisted of a number of sequences over 10 s parallel and 10 s perpendicular polarized emission, until a peak content in the data sets of 20 000 to 100 000 was reached, depending on the requirements. All measurements were followed by registration of the background fluorescence of the solvent for subtraction purposes. The absorbances of the samples were between 0.09–0.1. The instrument sensitivity on the polarization of the detected decays (the G factor) were checked by verifying the plateau of the emission anisotropy histograms for short-living fluorophores. For such fluorophores the emission anisotropy histograms plateau should be equal to zero, i.e. $r(t \rightarrow \infty) = 0$, if the G factor is determined correctly. The necessary corrections of the polarized decays have been done for all the polarized fluorescence decays discussed in this work. Before the experiments on DMABN, a proper detection aperture was selected from a series of independent time-resolved polarization experiments, in order to eliminate a possible systematic error during the experiments on DMABN. We found that a proper selection of the detection aperture was essential for the accuracy and reliability of further time-resolved studies with polarized light, discussed in this work.

In Figs. 1 and 2 we show the histograms of the emission anisotropy decays, $r(t) = (I_{\parallel}(t) - I_{\perp}(t))/(I_{\parallel}(t) + 2I_{\perp}(t))$, reconstructed from the detected polarized fluorescence decays for DMABN. The decays were collected at short and long emission wavelengths. In Fig. 1 we show the emission anisotropy histograms for DMABN at 55°C: (a), (b) in toluene (excitation at 300 nm, emission at 339 nm and 442 nm) and (c), (d) in *n*-butyl chloride (excitation at 295 nm, emission at 348 and 455 nm). Fig. 2 shows emission anisotropy histograms of DMABN in glycerol at 21°C, obtained from the polarized fluorescence decays detected at short-wavelength emission 348 nm (a) and long-wavelength emission 526 nm (b). Furthermore, in Fig. 2 we show the emission anisotropy histograms for the long-wavelength emission of DMABN in ethanol at 481 nm (c) and in propanol at 481 nm (d). In all the cases shown in Fig. 2 the excitation wavelength was 295 nm. The measurements on DMABN in ethanol and propanol were performed at a temperature of −55°C.

In Table 1 we show the initial values of the emission anisotropy histograms for the short and long emission wavelengths, obtained from the polarized fluorescence decays of DMABN in different solvents and at different temperatures.

3. Computer generated histograms of the polarized fluorescence and emission anisotropy decays

3.1. Polarized picosecond decays

Let us consider the energy levels scheme (A) shown in Scheme 1. Two excited states, 1* and 1**, are populated due to the absorption of the exciting light. State 2* is populated via state-to-state kinetic relaxation (it is a transient state). The reaction is reversible, in general. The rate constants k_1, k_{12}, k_2 and k_{21} describe the kinetics of the system. k_{IC} is the rate constant for the internal conversion process.

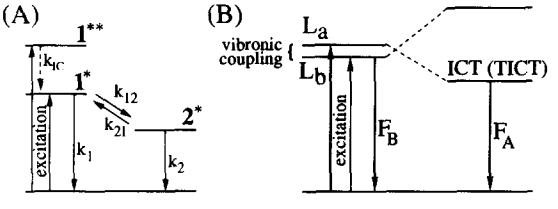

The polarized fluorescence decays relating to the situation depicted in scheme (A) are defined by the following relation [24,25]:

$$I_{\parallel(\perp)}(t, \lambda_{ex}, \lambda_{em}) = C(\lambda_{ex}, \lambda_{em}) \left(\omega^{(a)}(\lambda_{ex}) + \omega^{(b)}(\lambda_{ex})\right) \times \sum_{\xi=1,2} \kappa_{\xi}(\lambda_{em}) \left[\mathrm{Ph}^{(\xi)}(t) + \tfrac{4}{5}\left(-\tfrac{2}{5}\right) \phi^{(\xi)}_{(a,b)}(t)\right]. \quad (1)$$

$C(\lambda_{ex}, \lambda_{em})$ includes all excitation and emission wavelength-dependent instrumental factors. $\omega^{(a)}(\lambda_{ex})$ and $\omega^{(b)}(\lambda_{ex})$ represent the absorption bands to the

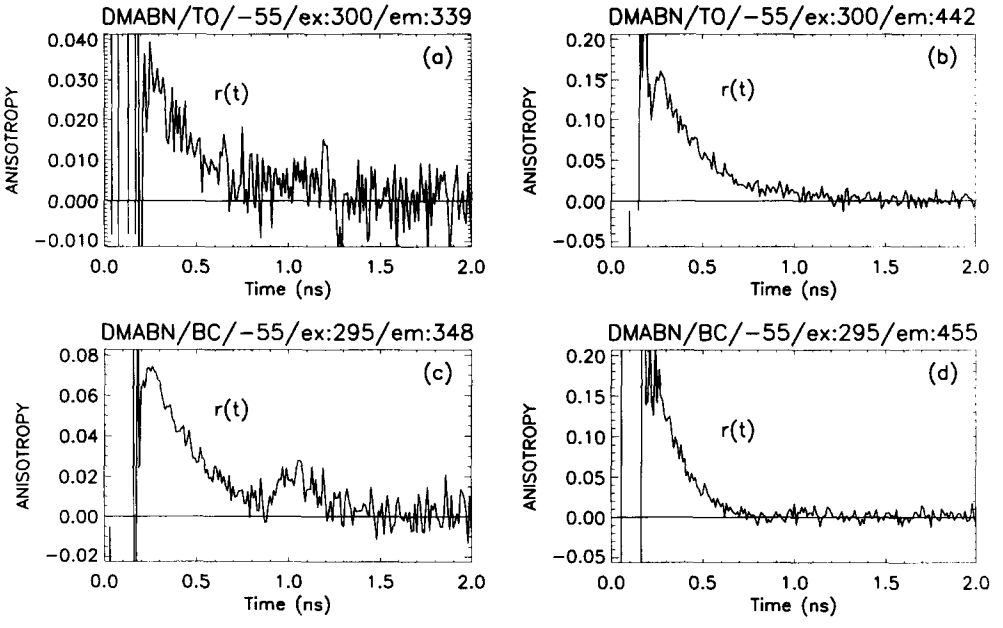

Fig. 1. DMABN at −55°C in: (a), (b) toluene (TO) and (c), (d) *n*-butyl chloride (BC).

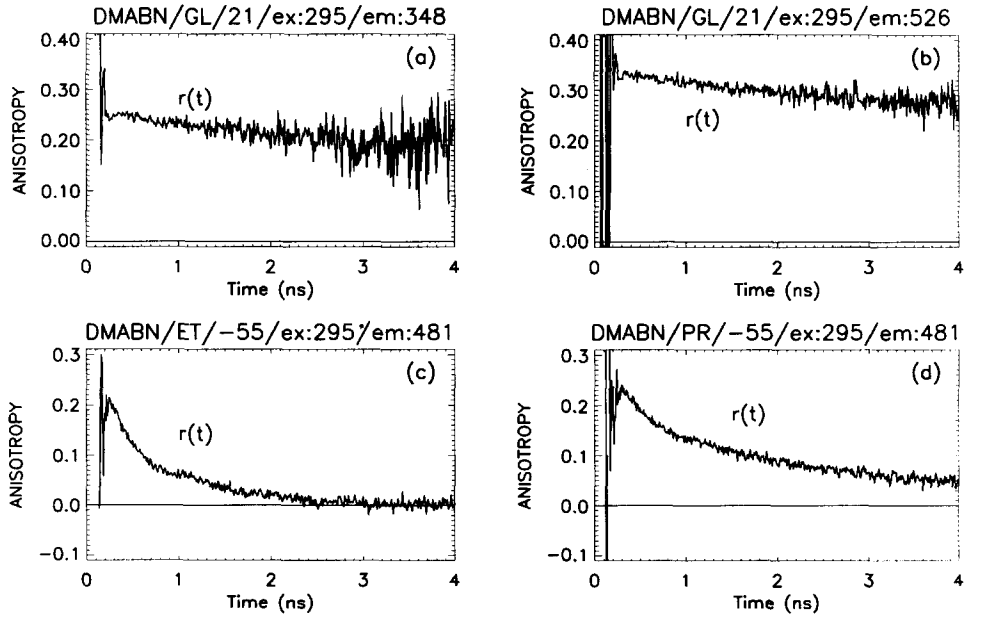

Fig. 2. DMABN in: (a), (b) glycerol (GL), (c) ethanol (ET) and (d) propanol (PR).

Table 1
Initial values of the emission anisotropy histograms of DMABN

Solvent	T (°C)	λ_{ex} (nm)	λ_{em} (nm)	$r(t \approx 0)$	λ_{em} (nm)	$r(t \approx 0)$	$\Delta\theta$ (°)
toluene	−55	300	339	0.03	442	0.15	22
n-butyl chloride	−55	295	348	0.07	455	0.16	21
butyronitrile	−30	300	349	0.11	466	0.20	17
butyronitrile	−55	300	349	0.13	466	0.22	15
acetonitrile	−30	300	349	0.13	526	0.24	13
ethanol	−55	295	348	0.07	481	0.21	16
propanol	−55	295	348	0.07	481	0.24	13
glycerol	21	295	348	0.25	526	0.34	0

excited states 1** and 1*, and $\kappa_\xi(\lambda_{em})$ ($\xi = 1,2$) represent the emission bands of excited states 1* and 2*, respectively. $\mathrm{Ph}^{(\xi)}(t)$ describes the kinetics of the system while $\phi^{(\xi)}_{(a,b)}(t)$ describes the kinetics coupled to the state-dependent rotational dynamics of symmetric rotors, and where

$$\mathrm{Ph}^{(\xi)}(t) = R^{(\xi)}_{00}(t), \tag{2}$$

$$\phi^{(\xi)}_{(a,b)}(t) = \sum_{q=0,1,2} R^{(\xi)}_{2q}(t) \times \left(c_a(\lambda_{ex}) T^{(a,\xi)}_q + c_b(\lambda_{ex}) T^{(b,\xi)}_q\right). \tag{3}$$

$c_i(\lambda_{ex})$ (i =a, b) are the relative spectral contributions of the constituent absorption bands at λ_{ex}, and

$$c_a(\lambda_{ex}) = \frac{\omega^{(a)}(\lambda_{ex})}{\omega^{(a)}(\lambda_{ex}) + \omega^{(b)}(\lambda_{ex})},$$

$$c_b(\lambda_{ex}) = \frac{\omega^{(b)}(\lambda_{ex})}{\omega^{(a)}(\lambda_{ex}) + \omega^{(b)}(\lambda_{ex})}, \tag{4}$$

where $c_a(\lambda_{ex}) + c_b(\lambda_{ex}) = 1$.

$T^{(i,\xi)}_q$ (i =a, b and $\xi = 1,2$) describe the angular dependences of the polarized decays on the orientations of the absorption and emission dipole moments in the molecule-fixed frame. They read

$$T^{(i,\xi)}_0 = P_2(\theta^{(i)}_A) P_2(\theta^{(\xi)}_E),$$
$$T^{(i,\xi)}_1 = \tfrac{3}{4} \sin 2\theta^{(i)}_A \sin 2\theta^{(\xi)}_E \cos(\varphi^{(i)}_A - \varphi^{(\xi)}_E),$$
$$T^{(i,\xi)}_2 = \tfrac{3}{4} \sin^2 \theta^{(i)}_A \sin^2 \theta^{(\xi)}_E \cos 2(\varphi^{(i)}_A - \varphi^{(\xi)}_E). \tag{5}$$

The polar angles $(\theta^{(i)}_A, \varphi^{(i)}_A)$ describe the orientations of the absorption transition dipole moments corresponding to the absorption bands $\omega^{(a)}(\lambda_{ex})$ and $\omega^{(b)}(\lambda_{ex})$, respectively. $(\theta^{(\xi)}_E, \varphi^{(\xi)}_E)$ define the directions of the emission transition dipole moments of excited states 1* and 2*. The $R^{(\xi)}_{jq}(t)$ appearing in (3) and (3) are given by the following relations:

$$R^{(1)}_{jq}(t) = A_{jq} \exp(-L^{(1)}_{jq} t) - B_{jq} \exp(-L^{(2)}_{jq} t),$$
$$R^{(2)}_{jq}(t) = k_{12} \left[\exp(-L^{(2)}_{jq} t) - \exp(-L^{(1}_{jq} t)\right] / \sqrt{\Delta_{jq}}, \tag{6}$$

where

$$L^{(1)}_{jq} = \tfrac{1}{2}\left(U^{(1)}_{jq} + U^{(2)}_{jq} + \sqrt{\Delta_{jq}}\right),$$
$$L^{(2)}_{jq} = \tfrac{1}{2}\left(U^{(1)}_{jq} + U^{(2)}_{jq} - \sqrt{\Delta_{jq}}\right), \tag{7}$$

$$A_{jq} = \frac{\left(U^{(1)}_{jq} - U^{(2)}_{jq} + \sqrt{\Delta_{jq}}\right)}{2\sqrt{\Delta_{jq}}},$$

$$B_{jq} = \frac{\left(U^{(1)}_{jq} - U^{(2)}_{jq} - \sqrt{\Delta_{jq}}\right)}{2\sqrt{\Delta_{jq}}}, \tag{8}$$

$$\Delta_{jq} = \left(U^{(1)}_{jq} - U^{(2)}_{jq}\right)^2 + 4W, \tag{9}$$

$$U^{(1)}_{jq} = j(j+1) D^{(1)}_{\parallel} + q^2 \left(D^{(1)}_{\perp} - D^{(1)}_{\parallel}\right) + U_1,$$
$$U^{(2)}_{jq} = j(j+1) D^{(2)}_{\parallel} + q^2 \left(D^{(2)}_{\perp} - D^{(2)}_{\parallel}\right) + U_2, \tag{10}$$

$$U_1 = k_1 + k_{12},$$
$$U_2 = k_2 + k_{21},$$
$$W = k_{12} k_{21}. \tag{11}$$

$D^{(\xi)}_{\parallel}$ and $D^{(\xi)}_{\perp}$ are the components of the state-dependent diffusion tensor for a symmetric rotor.

3.2. Synthetic data. Comparison with the experimental data

The synthetic data discussed in this section were generated on the basis of relation (1), adapted to the energy levels scheme of DMABN – see case (B) in Scheme 1. The absorption and emission bands, i.e. $\omega^{(a)}(\lambda_{ex})$, $\omega^{(b)}(\lambda_{ex})$, $\kappa_1(\lambda_{em})$ and $\kappa_2(\lambda_{em})$, used in the simulations are shown in Fig. 3(a). The absorptions bands A1 and A2 and the emission bands E1 and E2 have been simulated by using asymmetric Gaussian functions. The shapes and positions of the bands shown in Fig. 3(a) do not correspond to any particular experimental case for DMABN. The simulations discussed in this section have only a qualitative character. Nevertheless, the simulated absorption and emission bands are similar to those for DMABN in polar solvents at appropriate temperatures (e.g. see Ref. [10]). The same concerns the values of the state-to-state kinetic rate constants used in our simulations.

We assumed that the transition dipole moments of the bands A1 and A2 are polarized along the long and short molecular axes, respectively. The transition dipole moments of the emission bands E1 and E2 are directed along the short and long molecular axes, correspondingly. The positions of the emission bands E1 and E2 have been selected in such a way as to have a separate spectral access to the locally excited state and to the charge transfer state. The bands A1 and A2 correspond to the ^1L_a and ^1L_b absorption bands in DMABN. In Fig. 3(b) we show the steady-state polarization-free emission bands of both excited states, calculated from the relation $\int_0^\infty (I_\parallel(t, \lambda_{ex}, \lambda_{em}) + 2I_\perp(t, \lambda_{ex}, \lambda_{em}))\, dt$ for the rate constants $1/k_1 = 4$ ns, $1/k_{12} = 100$ ps, $k_2 = 8$ ns and $k_{21} = 800$ ps. The steady-state bands I_{E1} and I_{E2} correspond to the emission bands F_B and F_A, respectively, in the case of DMABN. In Fig. 3(c) we show the simulated polarization-free fluorescence decays. They have been obtained from the convolution of the model polarization-free decay, $I(t, \lambda_{ex}, \lambda_{em}) = I_\parallel(t, \lambda_{ex}, \lambda_{em}) + 2I_\perp(t, \lambda_{ex}, \lambda_{em})$, with the instrument response function $S(t)$, which in our case was given by a monoexponential fluorescence decay of xanthione in hexane (25 ps fluorescence lifetime) [25]. The fluorescence decays shown in Fig. 3(c) have been simulated for the excitation at 300 nm and for the emission wavelengths 370 (1), 460 (2) and 550 nm (3). The polarized fluorescence decays have been simulated for the following values of the state-dependent diffusion tensor components: $1/D_\parallel^{(1)} = 400$ ps, $1/D_\perp^{(1)} = 600$ ps, $1/D_\parallel^{(2)} = 700$ ps and $1/D_\perp^{(2)} = 1300$ ps (we assumed that the rotational motion of molecules in state 2* (F_A emission) is slower due to the stronger solute–solvent interactions in this state, as compared to state 1* (F_B emission)). The model decays (1) have been convoluted with the instrument response function $S(t)$. The Poisson noise has been added to the simulated polarized decays. All the calculations and the graphics presentation of the obtained results have been done in IDL (Interactive Data Language, Research Systems, Inc. (RSI), Boulder).

In Fig. 4 we show the final results of the simulations performed. Two cases were considered, namely: case (I), in which no vibronic mixing between the polarizations ^1L_a and ^1L_b was assumed, and case (II), in which this mixing was included by assuming that an "effective emission dipole moment" at short emission wavelengths makes an angle $\theta_E^{(1)} = 45°$ with the long molecular axis.

In case (I) the contribution of the A2 absorption band to the F_A emission was neglected and the condition $\omega^{(b)}(\lambda_{ex}) = 0$ was set, according to the energy level assignment for DMABN (assumed in the literature) in which the higher excited state ^1L_a is the precursor for the ICT (or TICT) state. As seen from Figs. 4(Ia,Ib), for the short emission wavelengths the emission anisotropy histogram takes negative values at initial time moments. This corresponds to the situation when the emission anisotropy decay originates from the z-polarized absorption and x-polarized emission (with a small contribution of the emission from the molecules which have been excited to S_1 – x-polarized absorption and x-polarized emission). At long emission wavelengths, where the emission anisotropy decay originates from the z-polarized absorption and z-polarized emission, the values of $r(t)$ are positive and $r(t \approx 0) \approx 0.4$ (see Fig. 4(If)).

In case (II) we assumed that vibronic coupling between states 1* (L_b) and 1** (L_a) occurs, leading to vibronically mixed polarization of the F_B emission. We assumed, in the calculations, that an effective emission oscillator makes an effective angle of 45° with the z-axis. Note that a mixed polarization of state 1* means that apart from the (normal) x-polarized

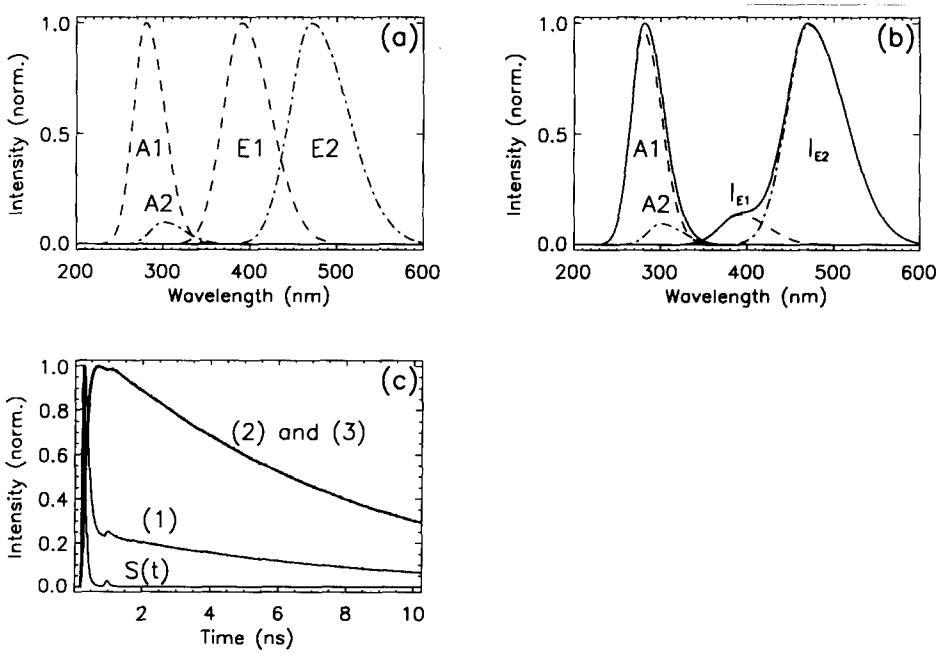

Fig. 3. The absorption and emission bands assumed in the computer calculations (a) and the calculated steady-state emission bands of both excited states (b). In (c) we show the kinetic decays for the excitation at 300 nm and the emission wavelengths 370 (1), 460 (2) and 550 nm (3). $S(t)$ represents the monoexponential fluorescence decay of xanthione in hexane (lifetime 25 ps).

emission component, also a z-polarized component of the emission occurs, which is vibronically "transformed" into state 1* from state 1**. (For the simplicity of the calculations, we did not account for the emission-wavelength dependence of this effect, see Refs. [7,9].)

The shape of $r(t)$ shown in Fig. 4(IIb) corresponds well to those observed for DMABN in toluene and *n*-butyl chloride (see Fig. 1) and also to all other cases shown in Table 1. Therefore, the initial values of the emission anisotropy histograms for the short emission wavelengths listed in Table 1 reflect the vibronic mixing of the close-lying states L_a and L_b, leading to a vibronically mixed polarization of the F_B emission. Synthetic data corresponding to the case of DMABN in glycerol (and other solvents, see Table 1) can be obtained by assuming a larger value of the angle between the effective emission oscillator and the long molecular axis, and by assuming a correspondingly slower rotational motion of the DMABN molecules.

The initial values of the emission anisotropy histograms for the long-wavelength emission, shown in Figs. 1, 2 and in Table 1, are much below the expected value 0.4, assuming that the F_A emission band is of A symmetry (^1L_a-type state). If the absorption and emission dipole moments are both parallel to the long molecular axis, the initial values of the emission anisotropy should be close to 0.4, according to Fig. 4(If). The low initial values of the emission anisotropy histograms for the long emission wavelengths, for the cases shown in Table 1, can result from a rapid reorientation of DMABN due to internal twisting of the amino group in this molecule. Such a molecular reorientation can decrease the initial value of the emission anisotropy, taking into account that the emission is detected from the twisted form of DMABN. Assuming that the absorption dipole moment in DMABN is oriented parallel to the z-axis, the reorientation of DMABN due to internal twisting cannot proceed around the z-axis alone, because such a reorientation will not depolarize the fluorescence even if the emission dipole moment is not directed along

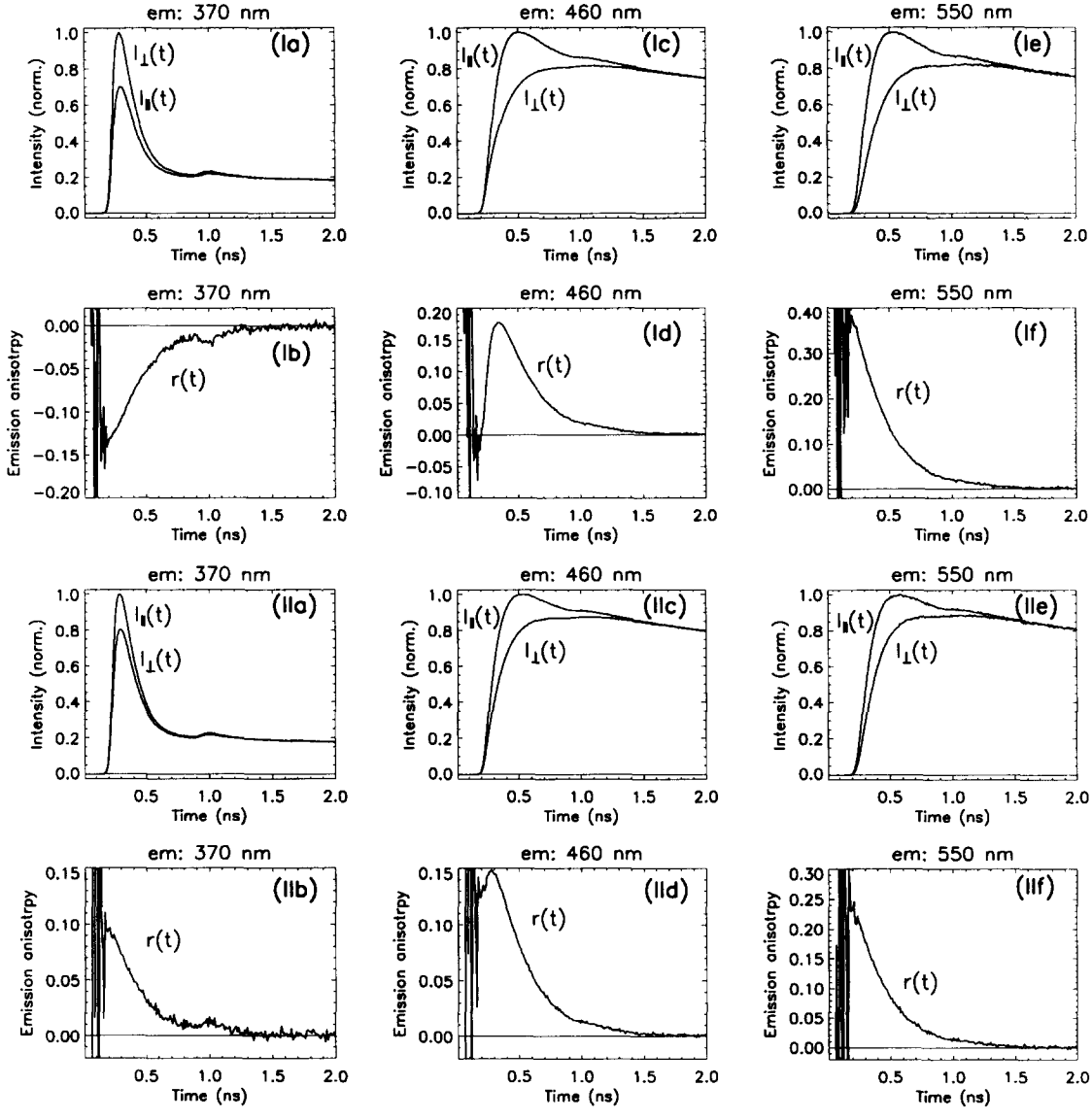

Fig. 4. The simulated polarized fluorescence and emission anisotropy decays. Case (I): the emission dipole moment in band I_{E1} is polarized along the short molecular axis (Ia-If). Case (II): due to vibronic mixing the effective emission dipole moment in band I_{E1} is polarized between the short and long molecular axes ($\theta_E^{(1)} = 45°$) (IIa–IIf).

the z-axis of DMABN. The reorientation of DMABN around its short axis, due to internal twisting of the amino group, is required to observe lower initial values of the emission anisotropy.

On the other hand, however, a relatively low initial value of $r(t)$ in the case of glycerol, $r(t \approx 0) \approx 0.34$, cannot be explained by this effect alone, due to the high viscosity of glycerol. Probably, the emission dipole moment of DMABN in the F_A emission band is not parallel to the long axis (z-axis) of DMABN. This could indicate a lower (effective) symmetry of DMABN in the charge transfer state. Assuming that the reorientation of DMABN forced by the internal twisting does not depolarize the fluorescence (or if

such a reorientation occurs, it proceeds around the long molecular axis alone and the absorption dipole moment is directed along the long axis of DMABN), from the initial value of the emission anisotropy the angle between the long molecular axis and the emission dipole moment in the F_A emission band, $\theta_E^{(2)} \approx 18°$, can be calculated. Nevertheless, even in the case of glycerol a fast depolarizing reorientation of DMABN due to internal twisting cannot be excluded from the considerations without further experimental studies.

In the computer simulations, in case (II), we assumed additionally that the emission dipole moment in the F_A emission band is not parallel to the long molecular axis of DMABN, and an angle $\theta_E^{(2)} \approx 30°$ was assumed. This assumption decreased the initial value of $r(t)$ to a value $r(t \approx 0) \approx 0.25$, according to Fig. 4(IIf). This value corresponds well to the initial values of $r(t)$ shown in Table 1 (excluding the case of DMABN in glycerol). Assuming that the value $\theta_E^{(2)} \approx 18°$ (obtained for DMABN in glycerol) is not affected substantially by the molecular reorientation of DMABN due to internal twisting, the value $\theta_E^{(2)} \approx 30°$ used in the computer calculations can be interpreted as being a sum of the angle $\theta_E^{(2)} \approx 18°$ and an angle $\Delta\theta \approx 12°$, where $\Delta\theta$ can be assumed as an (averaged) effective angle between the z-axis of DMABN before the internal twisting and the same axis just after the internal twisting of the amino group in this molecule. All the experimental cases listed in Table 1 can be interpreted in a similar way, and the calculated values of the angles $\Delta\theta$ will reflect the ability of DMABN for a reorientation due to the internal geometrical transformation in this molecule, in different solvents and at different temperatures. The values of $\Delta\theta$, calculated from the experimental data reported in this work, are listed in the last column in Table 1. It has to be emphasized here that the values of $\Delta\theta$ have been calculated under the assumption that the contribution of the F_B emission band to the fluorescence signals detected at long emission wavelengths, for the cases listed in Table 1, is negligible. The contribution of the F_B fluorescence will decrease the initial values of $r(t)$ (see cases (Id) and (IId) in Fig. 4), because the initial values of $r(t)$ take much lower values in the F_B emission band.

Although the considerations presented here do not provide any exact information on the orientation of the emission dipole moment in DMABN in the charge transfer state and on the change in orientation of the z-axis of DMABN due to internal twisting, the qualitative analysis demonstrated here can be a useful method for further more systematic experimental studies of the fluorescence depolarization of DMABN in the F_A emission band.

4. Discussion

The emission anisotropy histograms discussed in this work manifest a vibronic coupling mechanism in the short-wavelength (F_B) emission band of DMABN, which is in excellent agreement with the conclusions drawn in Ref. [7] and further confirmed in Ref. [9].

The long-wavelength initial values of the emission anisotropy histograms take lower values as compared to what one could expect taking into account the literature assumptions that the long-wavelength emission band originates from the L_a-state molecules and that the absorption and emission dipoles are mutually parallel for the fluorescence detected in the F_A band. On the basis of the experimental data reported in this work we concluded that probably internal twisting of the amino group in DMABN leads to a reorientation of the long axis of DMABN. The result observed for DMABN in glycerol seems to provide indication that the emission dipole moment in the F_A emission band is not directed along the long axis (the z-axis) of DMABN. Both effects may be responsible for much lower initial values of the emission anisotropy histograms, observed in this work. Undoubtedly, further, more systematic, fluorescence polarization studies of DMABN and other similar compounds are needed to explore this problem in more detail. First of all, the reason why the emission dipole moment in the F_A emission band is not parallel to the z-axis of DMABN, has to be indicated. It seems that the picosecond excitation and emission multiwavelength fluorescence polarization experiments performed on DMABN in different solvents and at different temperatures can display the discussed problem in more detail. Such experiments, apart from the qualitative analysis employed in this work, could be a subject of a more detailed analysis based on the formalism described in our recent work [25], adapted to the energy levels scheme of

DMABN. From the global analysis of the excitation and emission multiwavelength polarized fluorescence decay surfaces, the values of the angles $\theta_E^{(1)}$, $\theta_E^{(2)}$ and the components of the diffusion tensors describing the rotational dynamics of DMABN in both excited states, can be recovered. $\theta_E^{(1)}$ should be a freely adjustable parameter for all excitation and emission wavelengths and their values should reflect a characteristic (for the vibronic coupling mechanism) dependence on the excitation and emission wavelengths. The angle $\theta_E^{(2)}$ can be freely adjustable or it can be linked over all emission wavelengths. It would be interesting to verify whether its values change upon a change in the emission wavelength. (If $\theta_E^{(2)}$ varies with the emission wavelength, this could mean that also in the F_A emission band a vibronic coupling between the TICT state (the L_a-type symmetry) and another close-lying state of different symmetry occurs.) From the analysis discussed here the components of the state-dependent diffusion tensor can also be determined, enabling the differentiation of the state-dependent solute–solvent interactions. Values of the angle $\Delta\theta$ describing the change in the orientation of the long axis of DMABN due to internal twisting of the amino group, listed in Table 1, have been calculated under the assumption that at long emission wavelengths only the F_A fluorescence is detected. The global analysis of the experiments suggested above will enable the selection of such emission wavelengths or, if the F_B and F_A emission bands overlap, to decompose the effective fluorescence signal into F_B and F_A contributions, and finally, to calculate the initial values of $r(t)$ for an arbitrary emission wavelength in the F_A emission band. Thus the possible influence of internal twisting of the amino group in DMABN on the initial values of $r(t)$ can be explored more precisely.

The experiments reported in this work and their qualitative analysis demonstrated can be a method to verify different models offered in the literature to explain the photophysical and photochemical properties of aminobenzonitriles, e.g. the TICT mechanism [6–8], solute–solvent exciplex formation [15,16], the so-called "pseudo-Jahn–Teller coupling effect" model [18,19] and the model assuming a bending of the cyano group [20]. All these models are based on different assumptions which can be verified by means of the time-resolved polarized fluorescence technique. In the case of the TICT model, such effects as the internal-twisting-induced rapid reorientation of TICT compounds, leading to lower initial values of the emission anisotropy in the F_A emission band, and state-dependent solvation effects, leading to different rates for rotational motion in the LE and TICT state, should be observed. The fluorescence polarization experiments performed at short emission wavelengths should display in more detail the role of the vibronic coupling mechanism in the charge transfer reaction (the model discussed in Refs. [18,19]).

In the model offered in Refs. [18,19] the proximity between the S_1 and S_2 levels is a requirement and the N-inversion of the amino group is a promoting mode for the charge transfer reaction. In Refs. [18,19] the "proximity" between the S_1 and S_2 states is concluded from the position of both absorption bands of the aminobenzonitriles. This model has been argued on the basis of the absence of the dual emission in 1-methyl-5-cyanoindoline (NMCI) and 1-methyl-6-cyano-1,2,3,4-tetraquinoline (NMCQ) in polar solvents. In these systems the 5-membered or 6-membered ring connecting the amino nitrogen with the phenyl group hinders: (a) internal twisting of the amino group within the TICT model [7] or (b) the nitrogen inversion within the model proposed in Refs. [18,19]. The absence of dual emission for NMCI and NMCQ in polar solvents due to hindered nitrogen inversion has been argued in Refs. [18,19] by the fact that for NMCB (7-membered ring connecting the amino nitrogen with the phenyl group) with a more flexible aliphatic ring dual emission in polar solvents occurs.

On the other hand, NMCI and NMCQ show biexponential fluorescence decays in toluene [17]. This observation cannot be explained either in terms of the TICT model or in terms of the model proposed in Refs. [18,19]. The fluorescence polarization of NMCI and NMCQ shows vibronically mixed character [7] (the same is seen for DMABN in toluene, see Fig. 1 in this work). Therefore, what is the reason why double emission (in the time-resolved experiments) occurs for NMCI and NMCQ in toluene? The charge transfer reaction (!) and solute–solvent exciplex formation has been suggested in Ref. [17] to explain this observation. But why is this mechanism not operative in polar solvents? Perhaps, an assumption that the charge transfer state can be trapped by a small-angle out-of-plane torsional mode (a small-angle twisting

mode) of the amino group and by a fast modification of the electric field configuration (which is generated by the electric dipole moments induced in the toluene molecules) could be a possible explanation as to why dual emission occurs for NMCI and NMCQ in toluene. Toluene is a non-polar but highly polarizable solvent (the electric dipole moment can be induced in any direction in toluene molecules). Perhaps, the time scale for a larger-angle torsional mode of the amino group in NMCB is long enough so that the torsional mode can be trapped (stabilized?) in polar solvents (by the relaxation of solvent molecules to an appropriate configuration) and dual emission occurs. Undoubtedly, further studies are needed to explain this problem.

It seems that the experiments on NMCI and NMCQ in toluene, similar to the experiments on DMABN described in this work could be a direct way of verifying the hypothesis drawn in this work that the internal twisting in DMABN can lower the initial values of the emission anisotropy in the F_A emission band. One may expect that the small-angle twisting modes of the amino group in NMCI and NMCQ will not influence the fluorescence polarization, in contrast to the 90° internal twisting of this group in DMABN.

Acknowledgements

We would like to thank the referee for helpful comments. This work was supported by the Committee for Scientific Research (KBN, Poland) within Project 2.P303.089.04 and by the Department of Molecular Physics at the Agriculture University in Wageningen.

References

[1] E. Lippert, W. Lüder and H. Boos, in: Advances in molecular spectroscopy, European conference on molecular spectroscopy, Bolonga, Italy, 1959, ed. A. Mangini (Pergamon, Oxford, 1962) p. 443.
[2] E. Lippert, W. Lüder, F. Moll, H. Nagele, H. Boss, H. Prigge and I. Siebold-Blankenstein, Angew. Chem. 73 (1961) 695.
[3] E. Lippert, in: Organic molecular photophysics, ed. J. Birks, Vol. 2 (Wiley, New York, 1975) p. 1.
[4] S. Suzuki, T. Fujii and K. Sato, Bull. Chem. Soc. Japan 45 (1972) 1937.
[5] S. Suzuki, T. Fujii, A. Imai and H. Akahori, J. Phys. Chem. 81 (1977) 1592.
[6] K. Rotkiewicz, K.H. Grellmann and Z.R. Grabowski, Chem. Phys. Lett. 21 (1973) 212.
[7] Z.R. Grabowski, K. Rotkiewicz, W. Rubaszewska and E. Kirkor-Kamińska, Acta Phys. Polon. A 54 (1978) 767.
[8] Z.R. Grabowski, K. Rotkiewicz, A. Siemiarczuk, D.J. Cowley and W. Bauman, Nuova J. Chim. 3 (1979) 443.
[9] W. Rettig, G, Wermuth and E. Lippert, Ber. Bunsenges. Phys. Chem. 83 (1979) 692.
[10] E. Lippert, W. Rettig, V. Bonacic-Koutecky, F. Heisel and J.A. Miehe, Photophysics of internal twisting, in: Advances in chemical physics, Vol. 68, eds. I. Prigogine and S.A. Rice (Wiley, New York, 1987) p. 1.
[11] T. Okada, Proc. Indian Acad. Sci. (Chem. Sci.) 104 (1992) 173.
[12] J. Herbich, J. Karpiuk, Z.R. Grabowski, N. Tamai and K. Yoshihara, J. Luminescence 54 (1992) 165.
[13] Z.R. Grabowski, Pure Appl. Chem. 65 (1993) 1751.
[14] J. Herbich, K. Rotkiewicz, J. Waluk, B. Andersen and E.W. Thulstrup, Chem. Phys. 138 (1989) 105.
[15] E.A. Chandross, H.T. Thomas, Chem. Phys. Lett. 9 (1971) 397.
[16] P.C. Weisenborn, A.H. Huizer and C.A.G.O. Varma, Chem. Phys. 133 (1989) 437 and references cited therein.
[17] U. Leinhos, W. Kühnle and K.A. Zachariasse, J. Phys. Chem. 95 (1991) 2013.
[18] K.A. Zachariasse, Th. von der Haar, U. Leinhos, A. Hebecker, U. Leinhos and W. Kühnle, Pure Appl. Chem. 65 (1993) 1745.
[19] K.A. Zachariasse, Th. von der Haar, U. Leinhos and W. Kühnle, J. Inf. Rec. Mats. 21 (1994) 501.
[20] A.L. Sobolewski and W. Domcke, Chem. Phys. Lett. 250 (1996) 428.
[21] R.M. Hochstrasser and C.A. Marzacco, in: Molecular luminescence, ed. E.C. Lim (Benjamin, New York, 1969) p. 631.
[22] K. Vos, A. van Hoek and A.J.W.G. Visser, Eur. J. Biochem. 165 (1987) 55.
[23] A. van Hoek and A.J.W.G. Visser, Appl. Optics 29 (1990) 2661.
[24] J.J. Fisz, Chem. Phys. 181 (1994) 425.
[25] J.J. Fisz, Chem. Phys. Lett. 262 (1996) 495.